Author(s): Anne Marie S. Niehaus, Dionisios G. Vlachos Jeremy S.
Edwards, Petr Plechac and Roger Tribe
Article Title: Microscopic Simulation of Membrane Molecule Diffusion on
Corralled Membrane Surfaces

Microscopic Simulation of Membrane Molecule Diffusion on Corralled Membrane Surfaces

Anne Marie S. Niehaus,* Dionisios G. Vlachos,* Jeremy S. Edwards,[†] Petr Plechac,[‡] and Roger Tribe[§]

*Department of Chemical Engineering, University of Delaware, Newark, Delaware; [†]Molecular Genetics and Microbiology, Cancer Research and Treatment Center, University of New Mexico Health Sciences Center, and Chemical and Nuclear Engineering, University of New Mexico, Albuquerque, New Mexico; [‡]Department of Mathematics, University of Tennessee, Knoxville, Tennessee; and [§]Mathematics Institute, University of Warwick, Coventry, United Kingdom.

ABSTRACT   The current understanding of how receptors diffuse and cluster in the plasma membrane is limited. Data from single-particle tracking and laser tweezer experiments have suggested that membrane molecule diffusion is affected by the presence of barriers dividing the membrane into corrals. Here, we have developed a stochastic spatial model to simulate the effect of corrals on the diffusion of molecules in the plasma membrane. The results of this simulation confirm that a fence barrier (the ratio of the transition probability for diffusion across a boundary to that within a corral) on the order of 10^3–10^4 recreates the experimentally measured difference in diffusivity between artificial and natural plasma membranes. An expression for the macroscopic diffusivity of receptors on corralled membranes is derived to analyze the effects of the corral parameters on diffusion rate. We also examine whether the lattice model is an appropriate description of the plasma membrane and look at three different sets of boundary conditions that describe diffusion over the barriers and whether diffusion events on the plasma membrane may occur with a physically relevant length scale. Finally, we show that to observe anomalous (two-timescale) diffusion, one needs high temporal (microsecond) resolution along with sufficiently long (more than milliseconds) trajectories.

INTRODUCTION

Signal transduction is typically initiated when a ligand (i.e., epidermal growth factor or heregulin) binds to a receptor (i.e., ErbB1 or ErbB2, respectively). The binding of a ligand to a receptor often leads to receptor dimerization and higher-order receptor clustering. The clustered receptors then initiate a signal transduction cascade (including receptor phosphorylation and recruitment of adaptor proteins, kinases, and other signaling proteins), which controls cellular physiology. For example, many signaling pathways lead to the activation of transcription factors that control genes involved in regulating cell division and differentiation (1,2). It has been shown that deregulation of signaling pathways (i.e., ErbB, TNFR) is involved in the ability of continuous cell division, evasion of cell death, angiogenesis, and formation of metastases to cause cancer (3). Specifically, studies of ovarian, cervical, bladder and esophageal cancers show that patients with increased expression of ErbB1 have lower survival rates than patients with normal ErbB1 expression levels (4).

Receptor dimerization and clustering are critical for the activation of signaling pathways of many growth factor receptors (e.g., ErbB1). The receptor monomers are usually incapable of signaling; it is dimerization that leads to the phosphorylation events that trigger the signaling cascades (such as the mitogen-activated protein kinase (MAPK) cascade activated by ErbB1). To efficiently signal, the receptors must be in a sufficiently high local concentration on the membrane surface for dimerization to occur. The receptor population is concentrated in small regions in the plasma membrane (5). The clustering of receptors thus leads to signal amplification because they are close enough to dimerize and share ligands (6). Due to the importance of receptor interactions in the plasma membrane, understanding the spatial-temporal dynamics of receptor diffusion is important.

Widely accepted for over 30 years, the fluid mosaic model of the plasma membrane describes the phospholipid bilayer in which globular proteins are suspended and can diffuse freely within the plane of the membrane surface (7). Experimental data, however, yield two observations that are inconsistent with the fluid mosaic model. Diffusion coefficients for proteins in artificial membranes are higher than those in a natural membrane by a factor between 5 and 50 (8). Also, the diffusion rates of receptor dimers are significantly lower than those of receptor monomers (8), even though doubling particle size should have only a small effect on diffusivity (9). Insights into these discrepancies have been provided by recent single-particle tracking experiments with 25-μs resolution, which have revealed that diffusion does not follow a Brownian motion as earlier experiments with 33-ms resolution indicated (10,11). Receptors and other membrane protein molecules are trapped within, and occasionally hop between, compartments (also called "corrals" here), which are separated by barriers (hereafter also called "fences") (8,10–17). These compartments range in size from 30 to 230 nm, and the average residence time of a molecule within a compartment ranges from 1 to 17 ms, depending on the cell type (11). It has been hypothesized that

membrane corrals are formed by interactions between membrane molecules and the cytoskeleton. Fences dividing the corrals are created either by steric hindrance due to the closeness of the actin cytoskeleton to the membrane (the membrane-skeleton fence model) (14), or by membrane proteins bound to the cytoskeleton between which diffusing particles must pass to diffuse to an adjacent corral (the protein picket model) (8). These fences and corrals may be the mechanism by which receptors are localized to specific areas of the plasma membrane, and an understanding of how these fences work could aid in designing new cancer therapies.

Due to the importance of the problem, stochastic Monte Carlo (MC) simulations have been performed to address various aspects of diffusion on corralled plasma membranes. These simulations revealed that diffusion consisting of infrequent intercompartmental hops can appear as slow Brownian motion if results are analyzed at a low data collection rate (10,18,19). Despite this knowledge, a theoretical framework for predicting the diffusion of receptors on a corralled plasma membrane is currently lacking. Several questions about the meaning of the experimental results remain unanswered. Are the microscopic (or macroscopic) diffusivities of particles on the membrane actually measured by single-particle techniques? Is the lattice model used in simulations an accurate representation of the plasma membrane? Can these membrane barriers lead to clustering of receptors? Understanding what factors control the macroscopic diffusivity on corralled membrane surfaces could lead to a more comprehensive analysis of the data.

In this work, we simulate diffusion on a membrane surface and obtain diffusivity results similar to those of Ritchie et al. (10). Furthermore, we derive an analytical expression for the diffusivity of particles on a corralled surface. We investigate the effect of the lattice constant on the diffusivity both in the simulation and in the derived expression to understand how the fences behave and explore various boundary conditions for jumps over fences. Finally, the theoretical formula is applied to diffusion data from single-particle tracking experiments to compare the membrane fences from various cell types.

METHODS

Kinetic Monte Carlo (KMC) simulation

For the majority of the simulations reported here, the plasma membrane was modeled as a square lattice with a lattice constant, a, which was chosen to be 6 nm, following the work of Ritchie et al. (10). The suitability of a lattice model is assessed in Appendix A, and the effect of lattice constant is thoroughly investigated below. Only a small portion of the plasma membrane was modeled, and periodic boundary conditions were used to represent the entire membrane. On a square homogeneous lattice, the diffusivity can be calculated from the equation (10,20)

$$D = a^2 \Gamma_d (1 - \theta),$$ (1)

where θ is the coverage (fraction of sites occupied by receptors), a is the lattice constant (lattice site-to-site distance), and Γ_d is the propensity or

transition probability per unit time for diffusion of a receptor in one direction. The propensity is equal to the inverse of the average time step for a given event for a single particle. For the parameters used here ($D = 9$ nm^2/μs; $a = 6$ nm (10)), $\Gamma_d = 0.25$ μs^{-1}. The coverage was chosen to be equal to 0.01 for the lattice constant of 6 nm, and the density of receptors was kept constant for simulations with varying lattice constant.

To simulate systems with barriers at regularly spaced intervals, a fence was added surrounding a simulated space, representing a corral. Diffusion across the periodic boundary was given a lower propensity for occurrence than normal diffusion. The ratio of the propensities for diffusion within a corral (Γ_d) to the propensity for diffusion across a boundary (Γ_f) is termed the fence barrier, R_b:

$$R_b = \frac{\Gamma_d}{\Gamma_f}.$$ (2)

A large fence barrier (e.g., 10^9) indicates a strong fence, where receptors rarely escape from their initial corral, whereas a smaller fence barrier (e.g., 10^1) indicates a weak fence. At the lower limit, $\Gamma_d/\Gamma_f = 1$, there is no fence (the mesh is completely homogeneous). For most simulations, a fence barrier value of 10^3 was used, corresponding to the hop probability of 0.0008 used by Ritchie et al. (10). Alternative boundary conditions are discussed in Appendices B and C.

The propensity for each event to occur must be normalized to a Γ_{max} value such that the total probability of an event occurring for any given receptor at any given site is ≤ 1. In the case of diffusion only, $\Gamma_{max} = 4 \times \Gamma_d$. In this algorithm, the probability of a specific event occurring (P_j) is

$$P_j = \frac{\Gamma_j}{\Gamma_{max}}, \Gamma_j = \left\{ \begin{array}{l} \Gamma_d, \text{not crossing a fence} \\ \Gamma_f, \text{ crossing a fence} \end{array} \right\}.$$ (3)

We use a modified null-event algorithm for the KMC simulations (21,22), which is briefly described next. In each iteration, a receptor is selected at random. A random number (from a uniform distribution) between 0 and 1 is used to select an event, in this case a direction for diffusion. If the random number is between 0 and $P_1 = \Gamma_1/\Gamma_{max}$, then direction 1 is selected; if the random number falls between $P_1 = \Gamma_1/\Gamma_{max}$ and $P_1 + P_2 = (\Gamma_1 + \Gamma_2)/\Gamma_{max}$, then direction 2 is selected, and so on for all four possible diffusion directions. In this way, the probability of a receptor diffusing in a given direction is weighted by the propensity for the given diffusive event to occur. If the site adjacent to the selected receptor in the randomly chosen direction is empty, the receptor is moved and the clock is incremented by an average time step of (the actual time increment is given from an exponential distribution)

$$\Delta t = 1 / \Gamma_{total},$$ (4)

where

$$\Gamma_{total} = \sum_{j=1}^{n} \sum_{i=1}^{4} \Gamma_{j,i} (1 - \theta_{j,i}).$$ (5)

For our simulations, $\Gamma_{j,i}$ is either Γ_d or Γ_f, depending on whether or not receptor j would cross a boundary by diffusing in the ith direction; n is the number of receptors; and $\theta_{j,i}$ is the occupancy of the ith neighbor site of receptor j ($\theta_{j,i} = 0$ if the site is empty, $\theta_{j,i} = 1$ if it is full). If the adjacent site is full or the random number is greater than the total of all the probability values, the event ends with no movement of receptors and the clock is not incremented (i.e., a null event occurs). After the execution (or nonexecution) of an event, a new receptor is selected, and the process repeats. Despite having null events for which the time clock is not updated, it can rigorously be shown that the null-event algorithm is equivalent to the more common rejection-free algorithm, where all events are successful and the time clock is updated at each event (23).

Diffusivity calculations

Locations of all receptors were recorded at regular intervals, with the interval chosen as the resolution of the simulation, similar to the time resolution of experimental data (8,10,11,17). From these positions, the mean-squared displacement (MSD) was calculated and averaged over all particles and starting times. The diffusivity is given by

$$D = \frac{1}{4} \lim_{t \to \infty} \frac{\langle x^2 \rangle}{t}. \tag{6}$$

The diffusivity was calculated by fitting points 2–4 on the MSD versus time (t) plot to a straight line, similar to the D_{2-4} described by Kusumi et al. (24). In the timescale of long simulations, the slope reached a constant value, which was assumed to be equal to the infinite time limit of MSD/t. Therefore, the long-timescale (macroscopic) diffusivity was calculated by dividing the slope by 4.

EFFECT OF BARRIERS ON DIFFUSIVE BEHAVIOR OF MEMBRANE RECEPTORS

Simulations of 100 receptors (1% coverage) diffusing within a 600×600 nm corral with a lattice constant of 6 nm, were run for fence barriers (R_b) between 10^9 and 1. The MSDs for these simulations are shown in Fig. 1. In the absence of a fence, the MSD varies linearly with time. An increase in R_b causes the MSD to decrease from this linear limit. In the limit of a zero probability of crossing a boundary ($R_b \to \infty$), the MSD reaches a maximum value and remains constant thereafter, making the diffusivity equal to zero.

At short times, the diffusivity is relatively unaffected by the presence of the barriers, as shown near the origin of Fig. 1. On the other hand, the barriers decrease the long-time diffusivity by several orders of magnitude. Fig. 2 shows the trends in b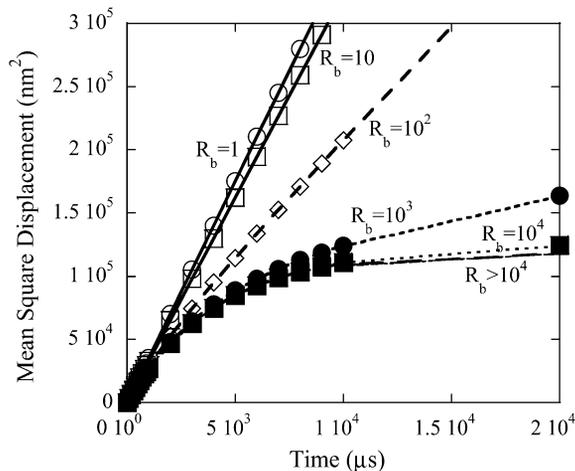oth the short- and long-time diffusivity calculated from the slopes in Fig. 1. The short-time diffusivity changes only slightly with changes in the fence barrier, whereas the long-time diffusivity decreases as the fence barrier increases. At short times, the receptors diffuse within the corral and do not interact with the barriers. As a result, the short-time diffusivity is close to the microscopic value of 9 nm^2/μs. At an R_b value of 10^3, the long-time diffusivity is 0.80 nm^2/μs, a factor of ~11 lower than the microscopic value. This ratio falls within the experimentally determined range of 5–50 for the difference in diffusivity between natural and artificial membranes (8). At very large values of R_b, the diffusivity is very low, and there are too few intercompartment hops in the simulation time used to accurately calculate the exact value. As a result, the diffusivity appears to plateau for $R_b > 10^6$, but as discussed later, this behavior results from poor sampling.

The KMC simulations of corralled diffusion recreate the appearance of Brownian motion at low frame rates, as was found experimentally (8,10,11,17), even though the diffusion is not Brownian.

Fig. 3 a shows the trajectory results from a simulation of a single receptor particle with a time resolution of 33 ms (corresponding to a video-rate experimental resolution) over a course of ~1 s; the motion of the particle appears to be Brownian. Fig. 3 b shows the results of the same simulation with a resolution of 25 μs. The hop-diffusion behavior of the receptor is evident from the boxes (representing corrals) created by the trajectory.

The results in Fig. 3 show that the two-timescale diffusion will only be observed if the time resolution of the trajectory is sufficiently high, of the order of microseconds, and the trajectory is sufficiently long. A lower resolution will yield a
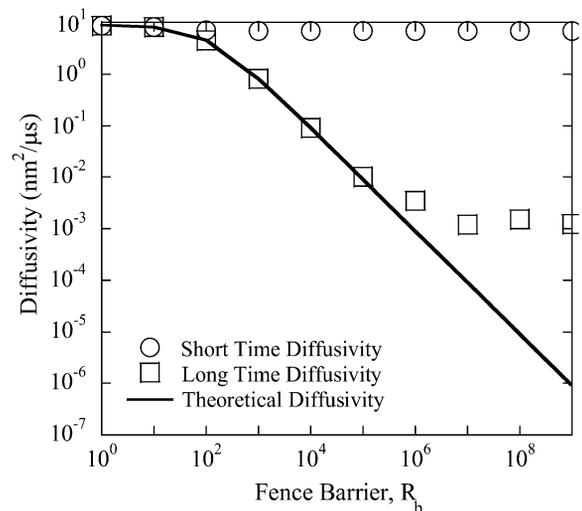

FIGURE 1 Mean-squared displacement curves for simulations of receptors diffusing on a membrane with a lattice of 600×600 nm corrals and fence barriers ranging from 1 to 10^9. (*Open circles*) $R_b = 1$ (no fence); (*open squares*) $R_b = 10$; (*open diamonds*) $R_b = 100$; (*solid circles*) $R_b = 10^3$; (*solid squares*) $R_b = 10^4$; curves with higher R_bs are indistinguishable from each other on this plot. Increasing the fence ratio (R_b) decreases the MSD at moderate to long times.

FIGURE 2 Long- and short-time diffusivities for simulations at various fence barrier values and a corral size of 600×600 nm. Short-time diffusivities are calculated at the first ~10^3 μs, and long-time diffusivities are calculated from simulation data collected between 2×10^4 and 1×10^5 μs. The theoretical diffusivity is obtained from Eq. 13. The deviation between the long-time diffusivity and the theoretical diffusivity is due to poor statistics of the KMC for large fence barriers.
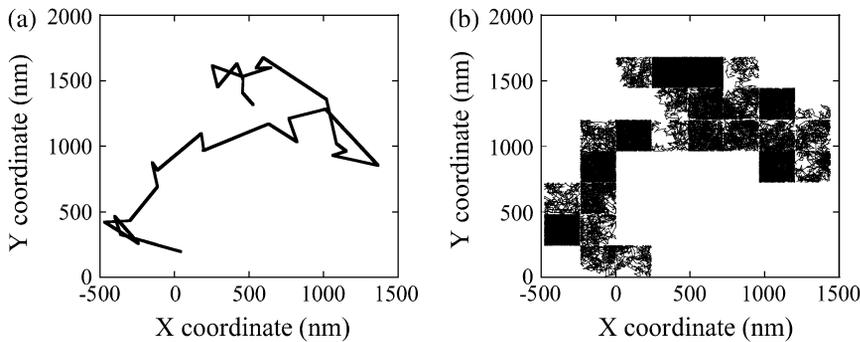
FIGURE 3 Single-particle trajectories from simulations with resolutions of (*a*) 33 ms and (*b*) 25 μs over a period of 1 s. Corral size is 240 nm $\times$ 240 nm and barrier height is $R_b = 10^3$. The diffusion in *a* appears to be Brownian, whereas in *b* it is corralled.

trajectory that appears as Brownian motion at the macroscopic diffusivity (see Fig. 3 *a*, Appendix D, and Figs. 13 and 14). This finding is consistent with experimental results at low resolution (at the millisecond timescale), where diffusion appears often to be simple (25–27). The results of Fig. 1 show that the trajectory must be followed for at least 5 ms to show hop diffusion. A shorter trajectory will appear as Brownian motion at the microscopic diffusivity. Appendix D provides more details about these time thresholds. The combination of high resolution and long trajectories means that simulations will be computationally expensive. For most simulations described in this work, simulations were run for a total time of 20 times the time resolution. The MSD was calculated for 10 time points from each simulation. For simulations where results for multiple timescales are given, the simulation was run for each timescale separately; then the results were compiled to complete the MSD (or diffusivity) plot. In this way, the high time resolution was used at short times, where it was required to compute the microscopic diffusivity within a corral, and to improve computational efficiency, a lower time resolution was used in creating trajectories long enough to show diffusion between corrals.

As is evident from the fact that not every ''box'' in Fig. 3 is full, the particle does not visit every site within a corral before moving to another corral, making it difficult to determine the exact size and shape of the corrals. This is also true in experimental systems (17). However, there is a relationship between the number of sites visited in a corral and the residence time (18). Because of these complications, the area visited by a receptor between intercompartment jumps must be assumed to be a lower limit on the size of a corral, not the actual size and shape of the corral.

EFFECT OF RECORDING RESOLUTION ON ESTIMATED DIFFUSIVITY

Current experimental techniques limit the time resolution of single-particle tracking to 25 μs. Murase et al. measured a diffusivity of ~5 nm^2/μs for particles diffusing within 200-nm corrals and estimated the diffusivity of liposomes to be ~10 nm^2/μs (11). Therefore, even at a 25-μs resolution, the measured short-term diffusivity appears to be approximately half of the true value. This introduces the question of what the

measured short- and long-time diffusivities really mean and whether, as experimental techniques improve, the true microscopic diffusivity of particles on a corralled membrane surface can ever be experimentally measured.

Simulations at varying timescales were carried out to estimate the potential capabilities of higher-resolution techniques. The diffusivity at a given resolution was calculated from the slope of the MSD at time points 2–4, as done by Murase et al. (11). Fig. 4 *a* shows the calculated diffusivities from these simulations for three different corral sizes.

All three curves in Fig. 4 *a* exhibit the interesting characteristic of an asymptotic limit at each end. At very short timescales, the measured diffusivity value is relatively constant and of the same order of magnitude as the microscopic diffusivity, because the receptors are unaffected by the presence of fences at these short timescales. In the transition region, the receptors are moderately affected by the fences. The ''bouncing'' of receptors back into their initial corrals decreases the rate of displacement from their initial positions. At long timescales, the receptors interact with the fences multiple times and the effective motion appears as a hop mechanism with a macroscopic diffusivity.

Fig. 4 *b* shows the MSD/4*t* at each data point from the simulation. The MSD/4*t* versus time plot appears similar to the diffusivity plot for the same corral sizes. At short times, the MSD is of the same order of magnitude for all corral sizes. However, at longer times, the results are affected by the corral size. The MSD/4*t* values deviate from each other more quickly for small corrals (42 nm) because the diffusing particles feel the effects of the boundaries sooner.

As expected, results from simulations taken at low resolution yield calculated diffusivities between 0.070 and 0.78 nm^2/μs (depending on the corral size), one or two orders of magnitude lower than the microscopic diffusivity of 9 nm^2/μs (see Table 1 for calculated diffusivity values). At these slow video rates, the diffusivity measured corresponds roughly to the macroscopic (infinite time) value (this is not exactly the case for large corrals, as Fig. 4 indicates). At the fast resolution rate of 25 μs, calculated diffusivities are between 0.46 and 7.1 nm^2/μs, on the same order of magnitude as the microscopic self-diffusivity, which supports the experimental evidence mentioned above. It is interesting that as the time resolution is improved, the diffusivity approaches an asymptotic limit less
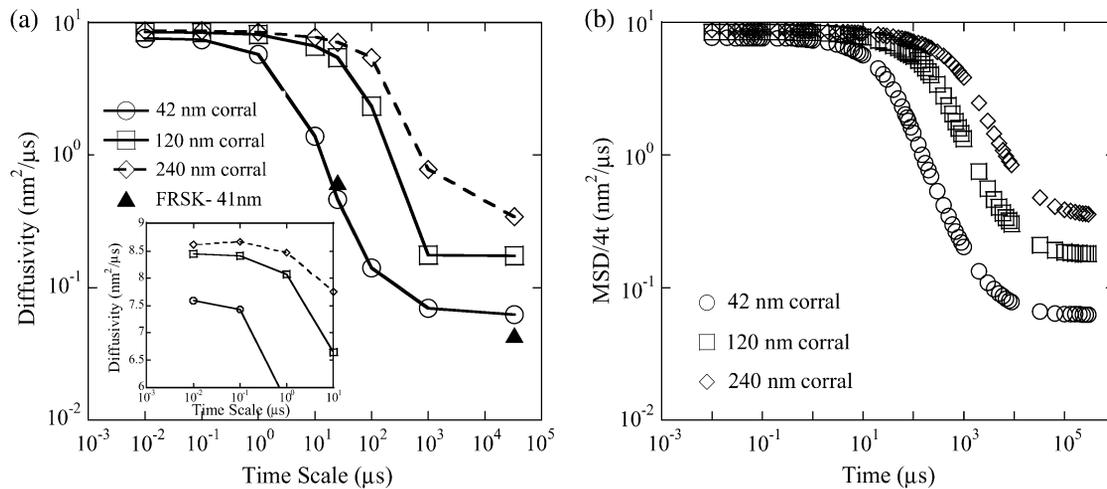
FIGURE 4 (*a*) Initial calculated diffusivity from points 2–4 taken at the intervals indicated. The average is taken over 10 simulations of 10,000 corrals with 1% coverage of receptors and a fence barrier value of $R_b = 10^3$, $D_{micro} = 9$ nm^2/μs. (*Open symbols* and *lines*) diffusivities calculated from simulation results; (*circles*) 42-nm corrals; (*squares*) 120-nm corrals; (*diamonds*) 240-nm corrals; (*solid triangles*) data from Murase et al. (11) for the measured diffusivity of particles on FRSK cells (average compartment size, 41 nm) at resolutions of 25 μs (fast resolution) and 33 ms (video rate). The inset is a blowup (in linear scale) of the short-term diffusivity. (*b*) Plot of MSD over four times the time (MSD/4t) for the same simulation results.

than the value of the microscopic diffusivity (Fig. 4 *a*, *inset*). Therefore, no matter how much the data collection rate for single-particle tracking improves, the measured diffusivity may be slightly less than the actual microscopic diffusivity. The reason for this is addressed below.

The short-timescale limit is closer to the microscopic diffusivity for larger corrals than for smaller corrals. This is expected, because as corrals become smaller, receptor movements more frequently sample the corral boundaries. Fig. 5 *a* shows the calculated diffusivity from simulation resolutions of 0.1 and 25 μs and varying corral sizes, along with experimental results from Murase et al. (11), whereas Fig. 5 *b* shows the MSD/4t for the same simulations. As corrals become large, the diffusivity approaches the microscopic diffusivity of 9 nm^2/μs. The agreement between the simulation and experimental data is fairly good.

AN ANALYTICAL EXPRESSION FOR THE MACROSCOPIC DIFFUSIVITY

In the simulations, for $R_b = 10^3$, there is a difference between Γ_d and Γ_f of three orders of magnitude (10). Thus, for every

intercompartmental hop, there are many events where a receptor is held in its corral by the boundary and even more events where a receptor merely diffuses from one mesh site to another within the corral. Therefore, most of the computational time is spent on fast events, and only a few slow events (hops over the fences) actually occur. As a result, it takes several hours to obtain results for diffusion of a single receptor over a time period of 10 s. It is clear that to efficiently simulate these systems, i.e., to treat the separation of timescales, coarse-graining is necessary. Coarse-graining will also be needed for incorporating more complexity, such as reactions, into the model and simulating an area of the cell surface larger than a few corrals. Therefore, a coarse-grained propensity must be derived that yields the same diffusivity results as the microscopic lattice simulations. An analytically derived expression for the coarse-grained diffusivity will also enable easy extraction of information from experimental data and a better understanding of the dependence of diffusivity on parameters, such as the corral size.

In our simulations, a coarse-grained lattice site was defined as the collection of all (q^2) microscopic lattice sites within a single corral (q is the size of the corral in each direction in lattice units). Several methods of coarse-graining on a two-dimensional lattice exist. A probability-weighted Monte Carlo simulation (22) determines the probability of leaving a coarse site by adding the propensities of all possible events and finding the fraction of events that lead to a coarse-grained event. The coarse-grained diffusion propensity can also be calculated by an equation derived by Chatterjee et al. (20) using nonequilibrium statistical mechanics coarse-graining theory for a uniformly coarse-grained lattice. Another method is to treat the boundary as a partially permeable membrane (28). Although all of these methods lead to a reasonable expression

TABLE 1 Short-time and long-time resolution diffusivity values from simulations with various corral sizes

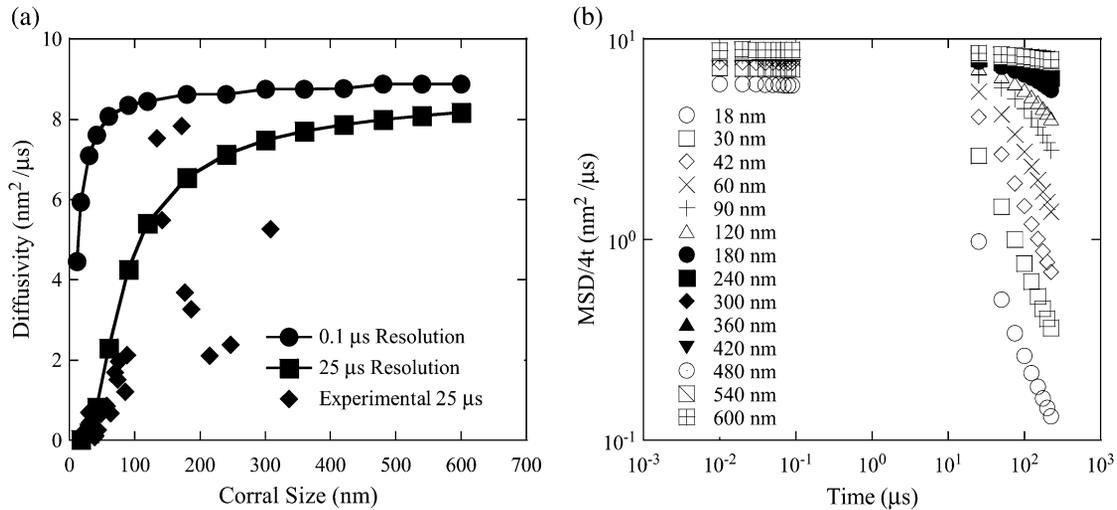| Corral size (nm)	0.01-μs resolution D (nm^2/μs)	25-μs resolution D (nm^2/μs)	1000-μs resolution D (nm^2/μs)	33-ms resolution D (nm^2/μs)
42	7.6	0.46	0.07	0.063
120	8.5	5.4	0.18	0.17
240	8.6	7.1	0.78	0.34

33 ms was the video resolution rate.

FIGURE 5 (a) Diffusivity calculated from simulation points 2–4 at a given resolution for receptors with a self-diffusivity of 9 nm^2/µs diffusing on a lattice of corrals with a fence barrier, R_b, of 10^3. Diamonds are experimental data from Murase et al. (11) measured by single-particle tracking with a resolution of 25 µs. (b) MSD over four times the time, MSD/4t, at each data point taken during simulations.

for the macroscopic diffusivity in some suitable limit, the equation derived using nonequilibrium statistical mechanics coarse-graining theory (20) gave the closest match to simulation results, and will be discussed here. The derivation below relies on the mathematically rigorous coarse-graining theory of microscopic processes on lattices we have been developing in recent years. A parity graph, discussed below, provides a visual assessment of the accuracy of our theoretical work.

The transition probability for diffusion along the x axis for a uniformly coarse-grained lattice from region (corral) k to region (corral) l is (20)

$$\Gamma_{\text{coarse}}(k \to l) = \frac{\Gamma_x}{2q^2} e^{-\beta U} \eta_k (1 - \theta_l), \quad (7)$$

where η_k equals the number of receptors in region k, q is the number of microscopic sites along one side of a corral, Γ_x is the propensity for diffusion from one microscopic site to a neighboring site, and θ_l is the coverage within region l, defined as the number of receptors in the region divided by the number of microscopic lattice sites. The exponential term is an energetic term representing the activation energy required for a particle to move between adjacent energy minima due to receptor-receptor interactions and is ignored hereafter because of the law density of receptors. Assuming a constant coverage, θ, from one corral to another (in the equilibrium limit), the expression simplifies to

$$\Gamma_{\text{coarse}} = \frac{N\Gamma_x}{2q^2}(1 - \theta) = \frac{N}{2}\frac{1}{\tau}(1 - \theta), \quad (8)$$

where N is the number of receptors in a single corral. The timescale for a single receptor to diffuse from one coarse lattice site to another depends on the coarseness and the transition probability, as follows:

$$\tau \propto \frac{q^2}{\Gamma_x}. \quad (9)$$

This expression applies to a uniform surface with no corrals or fences. To move from the center of one coarse region to the center of another, a receptor must make q steps in one direction. In a system with a fence at every coarse-grain boundary, $q - 1$ of these steps are within a corral, and one is a jump across a barrier. This must be incorporated into an expression for τ as a function of q, Γ_f, and Γ_d in such a way that the original expression is retained in the limit of $\Gamma_f = \Gamma_d$.

The timescale is split into two components, one corresponding to diffusion within a corral and the other to diffusion across the boundary between corrals. To accomplish this, one factor of q (representing the size of the corral in the direction of the fence hop) is separated into $q - 1$ and 1, whereas the other factor of q (representing the size of the corral in the perpendicular direction) is left alone. The following expression meets the aforementioned requirements:

$$\tau \propto \frac{q(q-1)}{\Gamma_d} + \frac{q}{\Gamma_f} = \frac{\Gamma_f q(q-1) + \Gamma_d q}{\Gamma_d \Gamma_f}. \quad (10)$$

Note that in the limit of $\Gamma_f = \Gamma_d$, the original expression for the timescale of diffusion on a uniform coarse-grained surface is recovered. Using this expression, the transition probability for diffusion from one corral to another is calculated from Eq. 8:

$$\Gamma_{\text{coarse}} = \frac{\frac{1}{2}\Gamma_d \Gamma_f}{\Gamma_f q(q-1) + \Gamma_d q} \times N(1 - \theta). \quad (11)$$

The general equation for the diffusivity on a lattice is

$$D = (aq)^2 \Gamma(1 - \theta). \quad (12)$$

Inserting the expression for Γ_{coarse} into Eq. 12 yields

$$D_{coarse} = \frac{a^2 q \Gamma_f \Gamma_d (1 - \theta)}{\Gamma_f (q - 1) + \Gamma_d}. \tag{13}$$

This equation can be rearranged to express the coarse diffusivity, D_{coarse}, in terms of the microscopic diffusivity instead of the microscopic transition probability. Equation 14 is the result of such a rearrangement:

$$D_{coarse} = \frac{D_{micro} q}{(q - 1) + R_b}, \tag{14}$$

where $D_{micro} = a^2 \Gamma_d (1 - \theta)$ is the microscopic diffusivity and R_b is the fence barrier. The corralled diffusivity varies directly with the microscopic diffusivity, and in the limit of very large q, it approaches D_{micro}. In other words, if the barriers are sufficiently far apart, diffusion is practically unaffected by barriers.

Fig. 6 compares the values for the diffusivity calculated using Eq. 13 to values obtained using KMC simulations (a parity graph) for a total of 19 simulations. The corral size (q), coverage (θ), frequency of diffusion (Γ_d), and frequency of jumping over a fence (Γ_f) were each varied to assess the accuracy of the theoretical expression on each parameter. The results show an almost exact correlation between the theoretical values and the simulation values.

The derived analytical expression for the macroscopic diffusivity shows that the diffusivity varies with R_b^{-1} when $R_b \gg q$. In the R_b range of interest, there is a difference between R_b and q of an order of magnitude or more, so this limit

applies. The solid line in Fig. 2 shows the theoretical result for long-time diffusivity decreasing with increasing R_b. The theoretical result is indistinguishable from the simulation at small to moderate fence barriers. The deviation between simulation and theory for large values of R_b is caused by the poor statistics (infrequent jumping over barriers) of the simulation. The derived expression (Eq. 14) accurately explains the previously determined macroscopic diffusivity.

This expression holds only for large timescales (e.g., >10,000 μs). This is because the coarse-graining produces an average of events occurring at short timescales and lumps them into a single diffusion event. This theoretical expression therefore does not capture the short-timescale microscopic and transitional diffusivities seen in Fig. 4 a. KMC simulations are necessary to compute diffusivities at short times.

EFFECT OF LATTICE CONSTANT ON DIFFUSIVITY

The expression for coarse-grained diffusivity derived above includes the parameter q, which is the number of lattice sites along the edge of a corral. This parameter depends on both the length of a corral and the length of a single lattice site ($q = L/a$, where L is the corral size, and a is the lattice constant). Kusumi's group chose a lattice constant of 6 nm so that the time step for a diffusive move would be 1 μs (10). However, the effect of the lattice constant on diffusivity is unclear.

A characteristic of the simulation results is the difference between the microscopic diffusivity value and the diffusivity calculated from the short-time simulation results (Fig. 4 a, inset). The smallest corrals contain only a few points and finite size effects can be important. For example, a lattice constant of 6 nm means that a 42-nm corral is modeled as a 7×7 square of lattice sites.

To determine whether the expression's dependence on the lattice constant is an artifact of the derivation or an actual representation of the simulation, simulations were run in which the lattice constant varied from its nominal value of 6 nm down to 0.01 nm. Diffusion propensities were recalculated from Eq. 1 for these simulations. The propensity for diffusion across a corral boundary (Γ_f) was chosen to keep R_b constant at 10^3. Therefore, the probability of a receptor next to a boundary jumping over a boundary rather than diffusing back into the same corral is the same for all simulations. Physically, this represents a fence with the same width as a lattice site, where the propensity for diffusing across it depends on its width. Diffusivity values calculated from these simulations are shown in Fig. 7. The results from short times indicate that decreasing the lattice constant does indeed bring the diffusivity closer to the microscopic limit of 9 nm²/μs. The long-time diffusivity is highly dependent on the lattice constant. The theoretical and simulated diffusivity values are given in Table 2.

Our simulation results are in good agreement with the theoretical diffusivity. As the lattice constant decreases, the
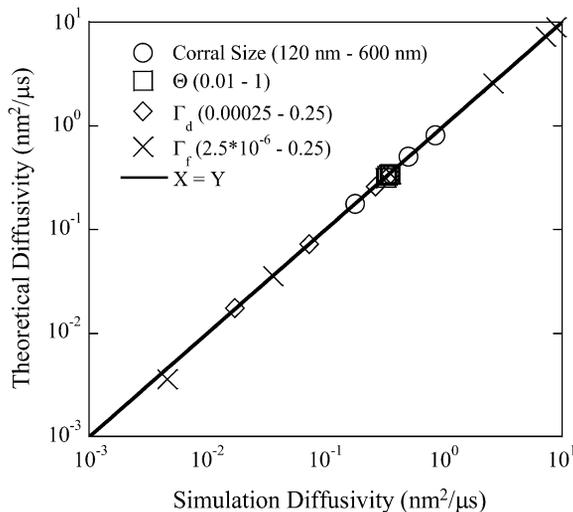

FIGURE 6 Parity plot comparing diffusivities obtained by simulation and calculated theoretically by the coarse-grained method. Results are averaged over 100,000 iterations for a single corral with periodic boundary conditions. Except for the parameter being varied, parameters are as follows: corral size, 240 nm × 240 nm; coverage, 0.01; $\Gamma_d = 0.25$; and $\Gamma_f = 0.00025$. Circles show variation in corral size (120–600 nm²); squares show variation in coverage (0.01–0.1); diamonds show variation in Γ_d (0.0005–0.25); and Xs show variation in Γ_f (0.25 × 10⁻⁶ to 0.25).
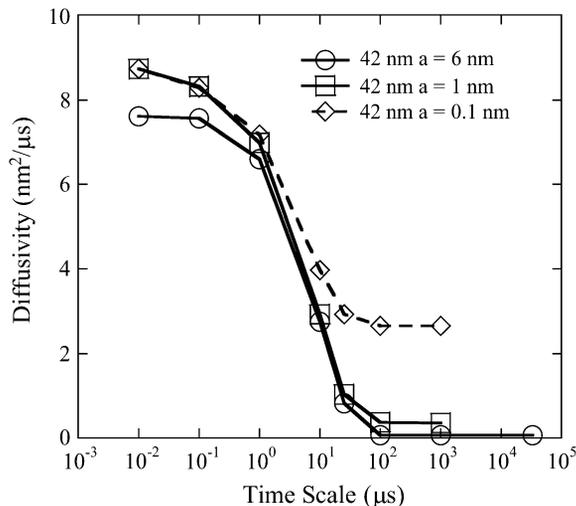
FIGURE 7 Diffusivity calculated at various timescales from simulations of receptors diffusing over 42-nm corrals with a fence barrier of $R_b = 10^3$ on a lattice of 0.1-, 1-, and 6-nm sites.

diffusivity increases. In the limit of $a \rightarrow 0$ ($q \rightarrow \infty$), D_{coarse} approaches the microscopic diffusivity:

$$\lim_{q \rightarrow \infty} D_{coarse} = \lim_{q \rightarrow \infty} \frac{D_{micro}q}{(q-1) + R_b} = \frac{D_{micro}q}{q} = D_{micro}. \quad (15)$$

This is because a hop from one corral to another is $q - 1$ hops within a corral and one hop across a corral boundary. As the lattice constant decreases, q becomes large, and the time for the many hops within a corral dominates over the time required for the single boundary hop. This occurs even though a boundary hop takes orders of magnitude longer than a single hop within a corral.

The dependence of the diffusivity on the lattice constant leads to the question of whether the lattice model accurately describes the plasma membrane system. Another model for the corrals is described in Appendix B, where the propensity for crossing a fence is kept constant (a fixed timescale for diffusion across a fence) when changing the lattice constant, and R_b is allowed to change. Off-lattice simulations, described in Appendix A, yield results matching those of lattice-based simulations for properly scaled values of time steps/lattice constant. Comparisons of the fence models in the main text and Appendix B with the off-lattice model in Appendix A

possibly indicate that the plasma membrane has a physically relevant length scale over which particles diffuse. Instead of a membrane protein or phospholipid being able to diffuse to any point on the surface of the membrane, the membrane consists of a lattice of likely positions. Diffusion behavior on the plasma membrane could take the form of phospholipids of finite size exchanging places with each other according to the milling crowd model (29). Because the membrane is crowded with phospholipids, the phospholipids themselves form a sort of lattice structure on the surface of the membrane. Although this lattice may be somewhat fluid, because the phospholipids are free to diffuse, it is no less capable of defining the length of individual diffusive events.

These results raise the question of whether it is mathematically possible to develop a lattice model (more specifically, suitable boundary conditions) in which, in the limit of the lattice constant going to zero, one gets the correct biological behavior, or whether the aforementioned milling crowd model is, conclusively, the only option. A third lattice model for diffusion simulations is described in Appendix C. In that model, the probability of a receptor at a fence boundary crossing into the next corral is proportional to the lattice constant. Such a method successfully models a macroscopic diffusivity that is independent of the lattice constant. In any event, the precise physics does not affect the analysis in our article, since the barrier remains within an order of magnitude as the lattice constant varies (see Fig. 10).

ANALYSIS OF EXPERIMENTAL DATA

The analytical expression for macroscopic diffusivity, derived above, was shown to closely describe the dynamics of the lattice-based simulation. To determine what insights can be gained from this analytical expression, it was applied to the experimental data obtained by Kusumi's group (11). Table 3 shows experimental data for the diffusivity and average

TABLE 2 Theoretical diffusivity and simulation diffusivity with a resolution of 1000 μs for a 42-nm corral length and a fence barrier of 10^3

Lattice constant, a (nm)	$q = L/a$ ($L = 42$ nm)	Theoretical diffusivity (nm^2/μs)	Simulation diffusivity (nm^2/μs)
6	7	0.0626	0.0623
1	42	0.363	0.361
0.1	420	2.66	2.65
0.01	4200	7.27	4.99

Theoretical diffusivity was calculated from Eq. 13.

TABLE 3 Diffusivity, compartment size, diffusion propensity, and fence barrier data of different cell types

Cell type	Diffusivity (nm^2/μs)	Compartment size (nm)	$\Gamma_f \times 10^4$ (1/μs)	Fence barrier, R_b
NRK	1.1	230	9.05	276
T24	0.17	110	2.62	953
HeLa	0.21	68	5.26	475
Hek293	0.38	68	9.69	258
PtK2	0.48	43	19.50	128
FRSK	0.19	41	7.87	318
HEPA-OVA	0.21	36	9.92	252
CHO-B1	0.24	32	12.78	196

Experimental data are from Murase et al. (11). Diffusivity was determined by single-fluorescent-molecule video imaging of Cy3-DOPE, and compartment size by single-particle tracking of gold-DOPE. A lattice constant of 6 nm and a microscopic diffusivity of 9 nm^2/μs were used. Γ_f was obtained using the coarse-grained diffusivity calculated according to Eq. 13. The average fence barrier is equal to 3.57×10^2.

compartment size in various cell types obtained by single-particle tracking techniques (11). Assuming a constant microscopic diffusivity allowed us to calculate Γ_f. This assumption implies that the structure of the plasma membranes of different cell types is similar except for the corrals. The Γ_f values calculated for each cell type's diffusivity and compartment size, according to Eq. 13, are given in Table 3.

All fence barriers are between 100 and 10^3, corresponding to the hop probability of 0.0008 used by Kusumi's group (10). Since the fence barriers are all of the same order of magnitude, it is concluded that the corrals are created by the same mechanism in all the cell types tested. The differences in cytoskeletal structure among the different cell types yield different compartment sizes due to actin filaments being closer together or farther apart; however, the fences themselves are probably similar in structure.

Given the dependence of the diffusivity on the lattice constant, the effect of the lattice on the analysis of Kusumi's experimental data was investigated. The calculated values of R_b for three values of the lattice constant are given in Table 4. The fence ratio, R_b, is seen to be inversely proportional to the lattice constant, a. Since the fence barrier is equal to the average number of times a molecule bounces off a barrier before passing through one, decreasing the lattice constant in simulations causes the receptors to hit and bounce off the barriers more often. If the fence barrier, R_b, has a physically meaningful value, there must also be a physically relevant value for the lattice constant, a, for the lattice model of the plasma membrane to be meaningful.

CONCLUSIONS

In this work, a stochastic spatial model was developed to describe the corralled diffusion behavior of molecules on the plasma membrane. These simulations confirm the hypothesis that corrals created by the actin cytoskeleton (or membrane proteins bound to it) can rationalize the difference between diffusivities in natural cell membranes and those in artificial membranes.

A theoretical expression for the diffusivity of corralled particles on a membrane surface as a function of corral size,

microscopic diffusivity, and fence barrier was derived using coarse-graining principles. This expression allows the prediction of macroscopic diffusivities at various values of the parameters, and an estimation of the fence barrier from experimental data of various cell types. Since similar values for the fence barrier were calculated for all cell types tested, it can be concluded that the physical basis of these fences is probably universal. What differs between cell lines is the structure of the overall cytoskeleton within the cell, and the distance between its filaments. This leads to the conclusion that cytoskeletal design is important not only for defining the structure of the cell as a whole, but also for controlling the diffusion of molecules on its surface.

The lattice constant has a great effect on the magnitude of the macroscopic diffusivity and the fence barrier. Both on- and off-lattice (Appendix A) models with constant fence barrier, R_b, and on-lattice models with constant timescale for a fence hop, Γ_f^{-1} (Appendix B), showed a strong dependence of the macroscopic diffusivity on the lattice constant. This could indicate that the plasma membrane actually behaves as a lattice with almost regularly spaced sites. The milling crowd model suggests that membrane particles diffuse by exchanging places with one another (29) and supports the idea of a lattice. This would mean that all diffusive moves are on the length scale of a single phospholipid molecule ($\sim$0.5 nm). Only the constant crossing probability per lattice size model (Appendix C) yields a diffusivity independent of the lattice constant. Although the exact nature of a fence is still unclear, it appears that the probability of moving across fences is 10^3–10^4 lower than moving within corrals. Further work is needed to elucidate details of the ''fence structures'' and obtain an even more atomistic view of such complicated diffusion phenomena. Finally, our simulations indicate that to observe anomalous (two-timescale) diffusion, one needs high temporal (e.g., microsecond) resolution along with sufficiently long (e.g., much greater than a millisecond) trajectories.

APPENDIX A: COMPARISON OF ON-LATTICE AND OFF-LATTICE SIMULATIONS

Since lattice simulations revealed that the lattice constant affects the macroscopic diffusivity, an off-lattice simulation was used to assess whether this behavior is a peculiarity of the lattice model. An algorithm for two-dimensional diffusion on a surface with regularly spaced fences was developed based on work by Higham (30) on Brownian motion (continuous in space and discrete in time).

Continuous-space algorithm

Higham's simulation method for Brownian motion uses a fixed time step for each event. Then, the displacement during that time step is normally distributed with a mean value of zero (27). The variance of the displacement is calculated from the microscopic diffusivity of the particles. Equation 6 gives the relationship between the MSD of a particle as a function of time and its diffusivity. Rearranged,

$$MSD = 4Dt. \tag{16}$$

TABLE 4 Values of the fence barrier (R_b) calculated for various lattice constant values

Cell type	$a = 6$ nm	$a = 1$ nm	$a = 0.1$ nm
NRK	276	1650	16,500
T24	953	5710	57,100
HeLa	475	2850	28,500
Hek293	258	1540	15,400
PtK2	128	764	7630
FRSK	318	1900	19,000
HEPA-OVA	252	1510	15,100
CHO-B1	196	1170	11,700

Experimental data used are from Murase et al. (11). Calculations were made using the coarse-grained expression for diffusivity (Eq. 13).

Since diffusion is isotropic, the displacement can therefore be separated into its components as follows:

$$MSD = \langle \Delta X^2 \rangle + \langle \Delta Y^2 \rangle = 4 \times D \times dt. \quad (17)$$

Since the x and y displacements have the same distribution,

$$\langle \Delta X^2 \rangle = 2 \times D \times dt. \quad (18)$$

For a distribution with mean zero, the expected value of x^2 is equal to the variance of the distribution. Therefore, the standard deviation is given by

$$\sigma = \sqrt{2 \times D \times dt}. \quad (19)$$

Simplified, the position of a receptor based on its previous position in one dimension is given by

$$X_{n+1} = X_n + (2D \times dt)^{1/2} N(0,1), \quad (20)$$

where $N(0,1)$ is the normal distribution with zero mean and variance 1.

Receptors are initially placed at random positions within a single corral using a uniform random number generator. In these off-lattice simulations, receptors are not affected by the presence of other receptors. Multiple receptors are used to obtain statistics.

During each time step, each receptor is moved once. For each move, two normal random numbers are generated with mean zero and variance as described above. These values determine the displacements in the x and y directions. If one of the random values is greater than the length of a corral (which occurs for <0.001% of events for 42-nm corrals if $dt < 6.1$ μs), the displacement in the corresponding direction is set equal to the length of a corral. The randomly generated displacements are added to the position of the receptor. If no fence is encountered in this displacement, the new coordinates of the receptors are saved, and the simulation moves to the next receptor.

When a receptor reaches a fence, the probability of jumping over it is P_{cross}, and the probability for bouncing away from it is equal to $1 - P_{cross}$. During a time step in which a particle encounters a wall, it moves a distance $(2D \times dt)^{1/2} N(0,1)$ with Prob. $= P_{cross}$, which corresponds to moving through the fence into another corral, or it moves a distance $X_{wall} - X_n$ toward the wall and a distance $(2D \times dt)^{1/2} N(0,1) - (X_{wall} - X_n)$ back from the wall with Prob. $= 1 - P_{cross}$, which corresponds to bouncing off the fence and back into its current corral. Displacements in the x and y directions are treated independently, so a receptor could encounter two walls in a given time step.

As in the lattice simulations, positions are recorded at predetermined time intervals and used to calculate the MSD over the time frame of the simulation. The slope of the MSD provides the diffusivity of the receptors.

Comparison between on- and off-lattice simulation results

Off-lattice simulations of diffusion of receptors on the corralled surface were run. Values of the time step were chosen so that the results could be directly compared to those of the lattice simulations. Results can be compared under the condition that the average distance traveled in a single time step is the same. In the off-lattice simulation, the average distance traveled during the time step dt is equal to

$$\sqrt{(\sqrt{2 \times D \times dt})^2 + (\sqrt{2 \times D \times dt})^2} = \sqrt{4 \times D \times dt}$$
$$= 2\sqrt{D \times dt}. \quad (21)$$

In the on-lattice simulations, the distance traveled by a receptor in a single event is designated a. Therefore, simulations where $a = 2\sqrt{D \times dt}$ can be compared to each other. This correlation can also be calculated from the equation for diffusivity on a lattice, $D = a^2 \Gamma_d (1 - \theta)$. If the coverage term is ignored (valid since the coverage is ~0.01), solving for the lattice constant gives:

$$a = \sqrt{D/\Gamma_d}. \quad (22)$$

In this case, Γ_d is equal to the inverse of the timescale for diffusion over a distance a in each of the four possible directions. Therefore, the timescale for diffusion in a single direction is equal to $(4\Gamma_d)^{-1}$. Thus, the lattice constant and timescale for a single event are related according to the expression

$$a = \sqrt{D/\Gamma_d} = \sqrt{D/(4dt)^{-1}} = \sqrt{4D \times dt} = 2\sqrt{D \times dt}. \quad (23)$$

This is the same expression derived above for the average step size for the off-lattice simulations.

In the lattice simulations, the fence barrier was used to define the probability of a receptor crossing a fence rather than remaining in its current corral. If a receptor is at a site next to a fence, the probability that the receptor leaves the corral and crosses the boundary is equal to $\Gamma_f/(\Gamma_d + \Gamma_f)$, and the probability that the receptor remains in the same corral is equal to $\Gamma_d/(\Gamma_d + \Gamma_f)$. Since Γ_f is two to three orders of magnitude less than Γ_d, the probability of a receptor at a boundary crossing the fence can be simplified to $P_{cross} = \Gamma_f/\Gamma_d = R_b^{-1}$.

In the off-lattice simulations, the probability of a receptor that encounters a fence crossing the fence, P_{cross}, is an input to the simulation. On- and off-lattice simulations can represent the same strength of the fence if the parameters are such that P_{cross} (off-lattice probability) is equal to R_b^{-1} (on-lattice fence barrier).

The diffusivities calculated from the off-lattice simulations are plotted together with the previously given results from lattice simulations in Fig. 8. All of these results are for a corral size of 42 nm and a fence barrier of 10^3. The off-lattice results match those of the lattice simulations for corresponding a and dt values. Also, decreasing the time step for a single event, like
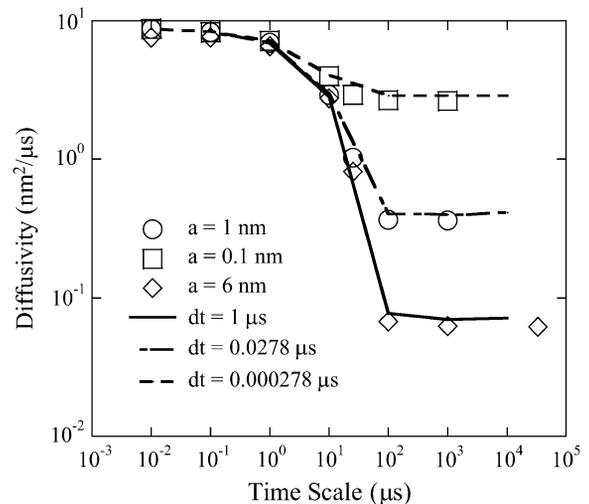

FIGURE 8 Diffusivity calculated from simulations of receptors diffusing on a surface with 42-nm corrals having an R_b value of 10^3. Symbols are results from lattice simulations with varying lattice constants, and lines represent results from off-lattice simulations with different time steps. Time steps of 1 μs, 0.0278 μs, and 0.000278 μs correspond to average step sizes of 6 nm, 1 nm, and 0.1 nm, respectively.

decreasing the lattice constant, increases the value for the macroscopic diffusivity.

Decreasing the time step for Brownian dynamics corresponds to decreasing the lattice constant for lattice random walk. Again, the number of steps needed to reach the fence increases, but the probability of jumping over the wall, P_{cross}, is kept constant. Since the time to move from one fence to the next remains constant, whereas dt for jumping across a fence decreases, the effect of fences on diffusivity also decreases. These simulation results show that discretizing in time rather than space does not change the effect of the step size on the calculated diffusivity.

APPENDIX B: AN ALTERNATIVE FENCE MODEL OF CONSTANT HOPPING TIME

In the above simulations, it has been assumed that the fence barrier remains constant. Another possibility is that the timescale for a fence hop is constant and independent of diffusion events within the corral. In this case, there would be an inherent length scale of the fence (its width), and the probability of crossing a barrier should depend on the lattice constant.

To implement this different concept of the timescale for diffusing across the fence, the propensity for diffusing within a corral is changed according to the lattice constant, with the propensity for diffusing across a boundary kept constant. Given that $q = L/a$, $R_b = \Gamma_d/\Gamma_f$, and $\Gamma_d = D_{micro}/a^2$, Eq. 14 can be rewritten as

$$D_{coarse} = \frac{D_{micro}La\Gamma_f}{(L - a)a\Gamma_f + D_{micro}}. \qquad (24)$$

In the limit of $a \to 0$, the numerator of this expression approaches zero while the denominator approaches D_{micro}. Therefore, the coarse-grained diffusivity approaches the microscopic diffusivity for constant R_b or zero for constant Γ_f.

Lattice-based KMC simulations were carried out with varying lattice constants and a constant value of Γ_f. Parameter values were chosen such that the simulations with a lattice constant of 6 nm are the same as those described earlier. The results from lattice-based simulations, where the propensity for crossing a barrier is held constant while the lattice constant changes, are shown in Fig. 9.

As in other simulations, the diffusivity at short timescales is close to the value of the microscopic diffusivity of 9 nm²/μs. The diffusivity approaches a macroscopic value asymptotically at long timescales. Unlike the results for constant R_b, as the lattice constant is decreased, the macroscopic diffusivity decreases and approaches zero. The simulation results shown in Fig. 9 indicate that the derived expression for macroscopic diffusivity is accurate in its description of the system's behavior at limiting values of the lattice constant. The results from this alternate model, together with the model presented in the text of this article, indicate that a characteristic length scale may exist in these systems or, possibly, that another physical model for fences is needed (see Appendix C).

APPENDIX C: AN ALTERNATIVE FENCE MODEL OF CONSTANT CROSSING PROBABILITY PER LATTICE SIZE

In previous sections, two models of hopping were studied. The first model in the text of this article included a constant fence barrier model, which gave a diffusivity approaching the microscopic diffusivity as the lattice constant became small. The second model (Appendix B) employed a constant propensity for fence hopping, which gave a diffusivity approaching zero as the lattice constant became small. In this appendix, we consider an alternative model in which a variable α, where
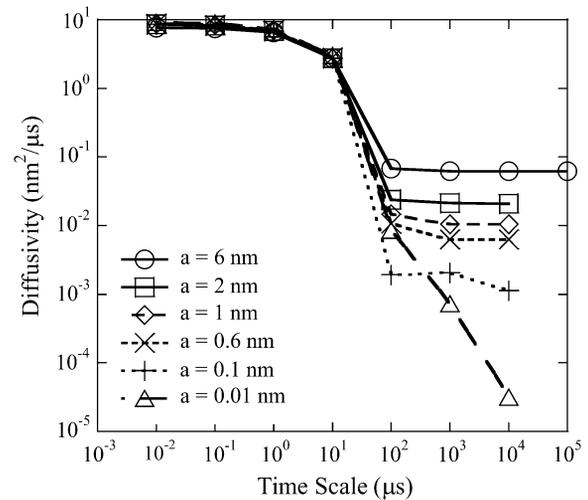

FIGURE 9 Diffusivities calculated from lattice-based simulations of receptors diffusing on a 42-nm corral with a constant propensity for crossing a barrier of 2.5×10^{-4} with $D_{micro} = 9$ nm²/μs.

$$\alpha = \frac{P_{cross}}{a}, \qquad (25)$$

is held constant. α is related to the permeability parameter described by Powles et al. (28). Here, P_{cross} is the probability of a receptor at a fence boundary crossing into the next corral and a is the lattice constant. By definition,

$$P_{cross} = \frac{\Gamma_f}{\Gamma_f + \Gamma_d}. \qquad (26)$$

A constant value of α means that the probability of a receptor crossing a fence into another corral is proportional to the size of the microscopic lattice sites. This scaling makes sense, because the time between microscopic moves decreases with the decreasing lattice constant. The specifics of the scaling are chosen in such a way that lattice constant independence is achieved in the limit where the lattice constant approaches zero. Thus, the smaller the distance between lattice sites, the more times a receptor will alternate between being next to the fence and being one lattice site away.

Comparison to other models

In the constant fence barrier model, R_b (Γ_d/Γ_f) is held constant. At the R_b value of interest (10^3 for $a = 6$ nm),

$$P_{cross} = \frac{\Gamma_f}{\Gamma_f + \Gamma_d} \approx \frac{\Gamma_f}{\Gamma_d} = \frac{1}{R_b}. \qquad (27)$$

Thus, in our previous model, holding R_b constant is the same as holding P_{cross} constant. In the new model, α is inversely proportional to the lattice constant. This implies that as the lattice constant becomes small, P_{cross} is disproportionately large.

In the case of the constant fence hop propensity model, Γ_f is held constant. The variable α can be estimated using

$$\alpha = \frac{P_{cross}}{a} = \frac{1}{a} \times \frac{\Gamma_f}{\Gamma_f + \Gamma_d} \cong \frac{1}{a} \times \frac{\Gamma_f}{\Gamma_d} = \frac{1}{a} \times \frac{\Gamma_f}{D_{micro}/a^2} = \frac{\Gamma_f a}{D_{micro}}. \qquad (28)$$

Since D_{micro} is constant and Γ_f is held constant, α is proportional to the lattice constant. Therefore, α decreases as the lattice constant decreases, and

the diffusivity would be expected to decrease to zero as the lattice size becomes infinitely small, in agreement with our simulations.

Parameter selection

The starting point for these simulations was a system with a lattice constant of 6 nm, a corral size of 42 nm, a microscopic diffusivity of 9 nm^2/μs, and a fence barrier of 10^3. This leads to a Γ_d of 0.25 μs^{-1} and a Γ_f of 0.00025 μs^{-1}. The value of α calculated from these parameters is 0.000167 nm^{-1} and is hereafter used so that mapping with the other models is possible. For each value of the lattice constant a, Γ_d and Γ_f are recalculated. The value of Γ_d is defined from the microscopic diffusivity and the lattice constant:

$$\Gamma_d = \frac{D_{\text{micro}}}{4a^2}. \tag{29}$$

Γ_f is then calculated using Eqs. 25 and 26:

$$\Gamma_f = \frac{\Gamma_d \alpha a}{1 - \alpha a}. \tag{30}$$

This expression was used to select the value of Γ_f for the simulations described below. Note that as the lattice constant changes, Γ_d and Γ_f vary according to Eqs. 29 and 30, respectively. The fence barrier in this case decreases with an increasing lattice constant, as shown in Fig. 10. However, for the changes in the lattice constant considered here, the fence barrier is within the range considered in the rest of this article.

Results

To assess whether this model actually yields diffusivity results independent of the lattice constant, simulations were done at decreasing lattice constants, with 42-nm corrals and a simulation space that is a square of 100×100 corrals with a total of 4900 receptors. This is equivalent to 1% coverage in the 6-nm lattice constant system. Diffusivities given are averaged over 100 runs.

Simulations were first run for a total time of 0.1 μs, and a data collection resolution of 0.01 μs. The results are shown in Fig. 11. A series of t-test analyses indicates that the diffusivity at each lattice constant is significantly different ($P < 0.01$). As the lattice constant decreases, the calculated diffusivity increases toward the microscopic value.
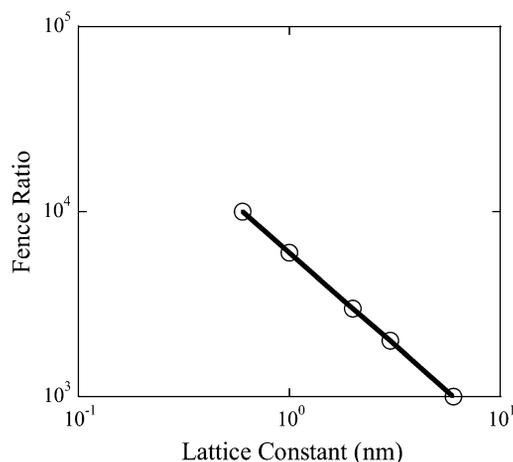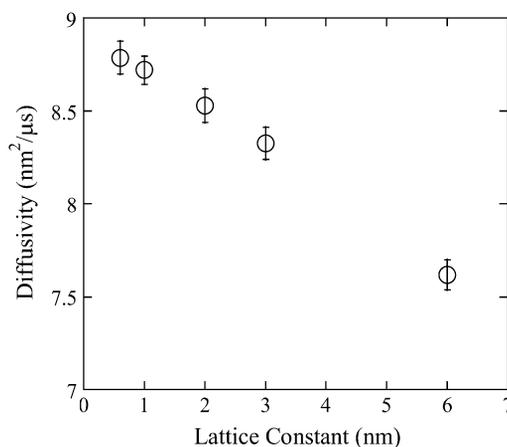

FIGURE 11 Diffusivity calculated at a time resolution of 0.01 μs versus the lattice constant. Error bars are standard deviations ($>$100 samples of 4900 receptors).

Similar simulations were run with a total time of 250 μs and a 25-μs resolution, equivalent to the resolution of fast single-particle tracking techniques. These results are shown in Fig. 12. At this time resolution, there is not a statistically significant difference between the diffusivities for lattice constants between 0.6 nm and 3 nm (a t-test yields P values $>$0.1).

From these results, it is concluded that deviations from the microscopic diffusivity in extremely short-time simulations are a consequence of finite size effects (large lattice constant with respect to the corral size). For longer time intervals, the diffusivity is fairly unaffected from the lattice constant. Mathematically, this new model gives a coarse diffusivity that is independent of the lattice constant as one passes to the continuum limit. It indicates that the boundary condition crossing the fence is an important issue that needs further work; for example, a more atomistic understanding of the fence structure and of the diffusion across a fence will be valuable in elucidating the mechanisms by which spatial self-organization may occur.

Coarse diffusivity

These results are compared to the previously derived expression for the coarse diffusivity on a corralled surface. Inserting the expression for the
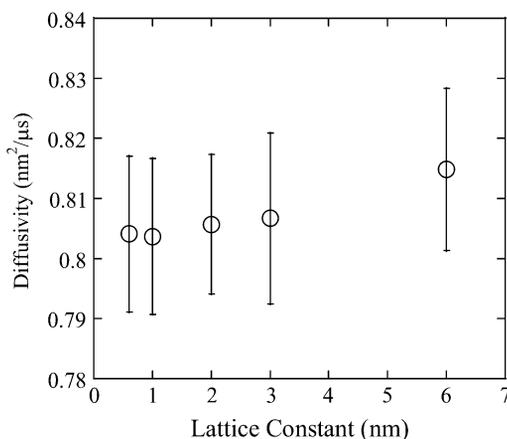

FIGURE 10 Variation of the fence barrier (Γ_d/Γ_f) with the lattice constant. Γ_d is calculated from Eq. 29 and Γ_f is calculated from Eq. 30.

FIGURE 12 Diffusivity calculated at a time resolution of 25 μs versus the lattice constant. At this timescale, the diffusivity is independent of the lattice constant. Error bars are standard deviations ($>$100 samples of 4900 receptors).
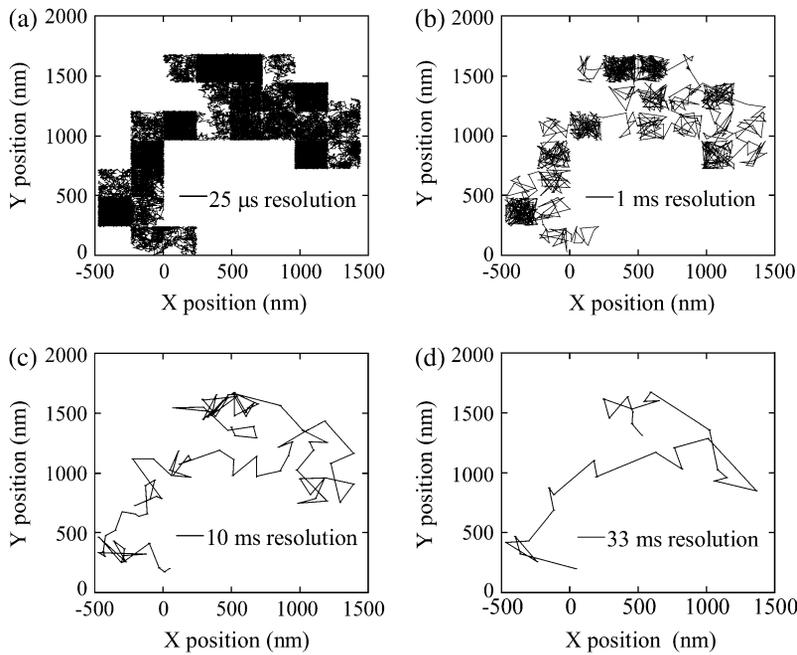
FIGURE 13 Trajectory plots for identical conditions with (*a*) 25-μs, (*b*) 1-ms, (*c*) 10-ms, and (*d*) 33-ms resolutions. Each trajectory is for a total time of 1 s.

propensity for a receptor to jump across a fence in terms of Γ_d, α, and a, the expression for the diffusivity is

$$D_{\text{coarse}} = \frac{D_{\text{micro}} L\alpha}{L\alpha - \alpha a + 1 - \alpha a} = \frac{D_{\text{micro}} L\alpha}{L\alpha - 2\alpha a + 1}. \quad (31)$$

In this expression, the lattice constant appears only in the denominator. In the limit of $a \ll L$, the dependence of diffusivity on the lattice constant becomes negligible. This relation also explains the results in Fig. 12, which show that the diffusivity with a lattice constant of 6 nm is slightly higher than the other diffusivities (with a lattice constant of 6 nm and a corral size of 42

nm, the lattice constant is less than an order of magnitude smaller than the corral, and the limit of $a \ll L$ does not apply).

APPENDIX D: TIME RESOLUTION NECESSARY FOR OBSERVATION OF HOP DIFFUSION

Figs. 13 and 14 show trajectories and MSDs for different time resolutions for our nominal simulation conditions. In Fig. 14, estimates of the diffusivity are also depicted. It is apparent that above a certain resolution threshold ($\sim$10 ms for our simulated conditions), there is no evidence in the trajectories of
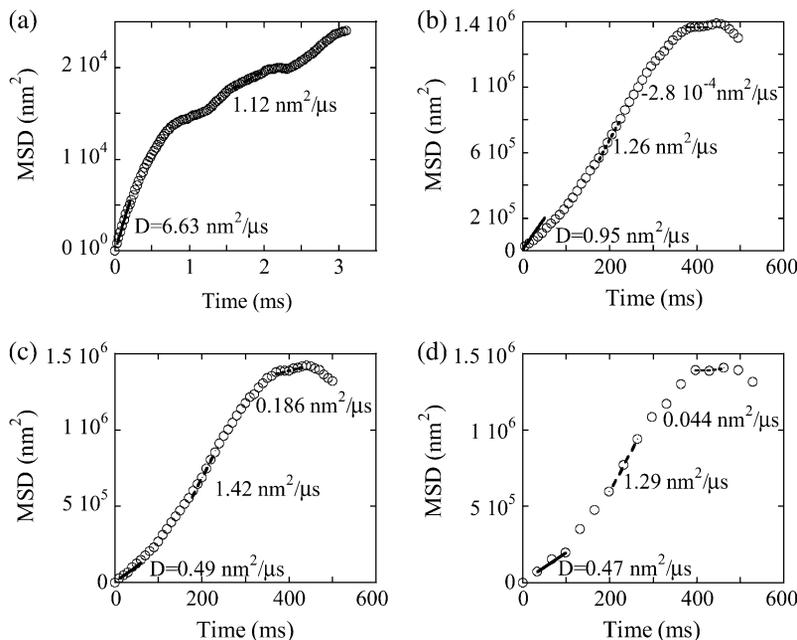

FIGURE 14 MSD plots for identical conditions with (*a*) 25-μs, (*b*) 1-ms, (*c*) 10-ms, and (*d*) 33-ms resolutions. (*a*) The diffusivities are given for time near zero and at 1.5 ms. (*b–d*) The diffusivities given are calculated from the slope of 3 points (indicated by lines) at time near 0, at $\sim$200 ms, and at $\sim$400 ms. The initial diffusivities are all calculated from points 2–4 in the plot. Only the data for 25 μs yield a diffusivity close to the microscopic value of 9 nm^2/μs.

two-timescale diffusion. In addition, only microsecond time resolution can provide a diffusivity that is close to the intrinsic microscopic one. Even at the 1-ms time resolution, the initial diffusivity is far from the actual one (lower by an order of magnitude). In addition, the estimated value of the initial diffusivity depends somewhat on the resolution employed. These threshold values will change somewhat depending on the specific cells, i.e., the exact values of the diffusivities, but are not expected to be drastically different from what has been found here for many cells.

REFERENCES

1. Johnson, G. L., and R. R. Vaillancourt. 1994. Sequential protein kinase reactions controlling cell growth and differentiation. *Curr. Opin. Cell Biol.* 6:230–238.

2. Saez-Rodrigues, J., A. Kremling, H. Conzelmann, K. Bettenbrock, and E. D. Gilles. 2004. Modular analysis of signal transduction networks. *IEEE Contr. Syst. Mag.* 24:35–52.

3. Holbro, T., G. Civenni, and N. E. Hynes. 2003. The ErbB receptors and their role in cancer progression. *Exp. Cell Res.* 284:99–110.

4. Nicholson, R. I., J. M. W. Gee, and M. E. Harper. 2001. EGFR and cancer prognosis. *Eur. J. Cancer.* 37:S9–S15.

5. Jorissen, R. N., F. Walker, N. Pouliot, T. P. J. Garrett, C. W. Ward, and A. W. Burgess. 2003. Epidermal growth factor receptor: mechanisms of activation and signaling. *Exp. Cell Res.* 284:31–53.

6. Ichinose, J., M. Murata, T. Yanagida, and Y. Sako. 2004. EGF signalling amplifications induced by dynamic clustering of EGFR. *Biochem. Biophys. Res. Commun.* 234:1143–1149.

7. Singer, S. J., and G. L. Nicolson. 1972. The fluid mosaic model of the structure of cell membranes. *Science.* 175:720–731.

8. Kusumi, A., C. Nakada, K. Ritchie, K. Murase, K. Suzuki, H. Murakoshi, R. S. Kasai, J. Kondo, and T. Fujiwara. 2005. Paradigm shift of the plasma membrane concept from the two-dimensional continuum fluid to the partitioned fluid: high-speed single-molecule tracking of membrane molecules. *Annu. Rev. Biophys. Biomol. Struct.* 34:351–378.

9. Saffman, P. G., and M. Delbruck. 1975. Brownian motion in biological membranes. *Proc. Natl. Acad. Sci. USA.* 72:3111–3113.

10. Ritchie, K., X.-Y. Shan, J. Kondo, K. Iwasawa, T. Fujiwara, and A. Kusumi. 2005. Detection of non-Brownian diffusion in the cell membrane in single molecule tracking. *Biophys. J.* 88:2266–2277.

11. Murase, K., T. Fujiwara, Y. Umemura, K. Suzuki, R. Iino, H. Yamashita, M. Sait, H. Murakoshi, K. Ritchie, and A. Kusumi. 2004. Ultrafine membrane compartments for molecular diffusion as revealed by single molecule techniques. *Biophys. J.* 86:4075–4093.

12. Edidin, M., S. C. Kuo, and M. P. Sheetz. 1991. Lateral movements of membrane glycoproteins restricted by dynamic cytoplasmic barriers. *Science.* 254:1379–1382.

13. Edidin, M., M. C. Zuniga, and M. P. Sheetz. 1994. Truncation mutants define and locate cytoplasmic barriers to lateral mobility of membrane glycoproteins. *Proc. Natl. Acad. Sci. USA.* 91:3378–3382.

14. Kusumi, A., and Y. Sako. 1996. Cell surface organization by the membrane skeleton. *Curr. Opin. Cell Biol.* 8:566–574.

15. Sako, Y., and A. Kusumi. 1995. Barriers for lateral diffusion of transferrin receptor in the plasma membrane as characterized by receptor dragging by laser tweezers: fence versus tether. *J. Cell Biol.* 129:1559–1574.

16. Sako, Y., A. Nagafuchi, S. Tsukita, M. Tateichi, and A. Kusumi. 1998. Cytoplasmic regulation of the movement of E-cadherin on the free cell surface as studied by optical tweezers and single particle tracking: corralling and tethering by the membrane skeleton. *J. Cell Biol.* 140:1227–1240.

17. Suzuki, K., K. Ritchie, E. Kajikawa, T. Fujiwara, and A. Kusumi. 2005. Rapid hop diffusion of a G-protein-coupled receptor in the plasma membrane as revealed by single-molecule techniques. *Biophys. J.* 88:3659–3680.

18. Saxton, M. J. 1995. Single-particle tracking effects of corrals. *Biophys. J.* 69:389–398.

19. Gheber, L. A., and M. Edidin. 1999. A model for membrane patchiness: lateral diffusion in the presence of barriers and vesicle traffic. *Biophys. J.* 77:3163–3175.

20. Chatterjee, A., D. G. Vlachos, and M. A. Katsoulakis. 2004. Spatially adaptive lattice coarse-grained Monte Carlo simulations for diffusion of interacting molecules. *J. Chem. Phys.* 121:11420–11431.

21. Lin, S. L., and J. N. Bardsley. 1978. The null-event method in computer simulation. *Comput. Phys. Commun.* 15:161–163.

22. Reese, J. S., S. Raimondeau, and D. G. Vlachos. 2001. Monte Carlo algorithms for complex surface reaction mechanisms: efficiency and accuracy. *J. Comput. Phys.* 173:302–321.

23. Chatterjee, A., and D. G. Vlachos. 2007. An overview of spatial microscopic and accelerated kinetic Monte Carlo methods. *J. Comput. Aided Mater. Des.* 14:253–308.

24. Kusumi, A., Y. Sako, and M. Yamamoto. 1993. Confined lateral diffusion of membrane receptors as studied by single particle tracking (nanovid microscopy). Effect of calcium-induced differentiation in cultured epithelial cells. *Biophys. J.* 65:2021–2040.

25. Vrljic, M., S. Y. Nishimura, S. Brasselet, W. E. Moerner, and H. M. McConnell. 2002. Translational diffusion of individual class II MHC membrane proteins in cells. *Biophys. J.* 83:2681–2692.

26. Wieser, S., M. Moertelmaier, E. Fuertbauer, H. Stockinger, and G. J. Schutz. 2007. (Un)confined diffusion of CD59 in the plasma membrane determined by high-resolution single molecule microscopy. *Biophys. J.* 92:3719–3728.

27. Lenne, P.-F., L. Wawrezinieck, F. Conchonaud, O. Wurtz, A. Boned, X.-J. Guo, H. Rigneault, H.-T. He, and D. Marguet. 2006. Dynamic molecular confinement in the plasma membrane by microdomains and the cytoskeleton meshwork. *EMBO J.* 25:3245–3256.

28. Powles, J. G., M. J. D. Mallett, G. Rickayzen, and W. A. B. Evans. 1992. Exact analytic solutions for diffusion impeded by an infinite array of partially permeable barriers. *Proc. R. Soc. Lond. A.* 436:391–403.

29. Eisinger, J., J. Flores, and W. P. Petersen. 1986. Milling crowd model for local and long-range obstructed lateral diffusion. *Biophys. J.* 49:987–1001.

30. Higham, D. J. 2001. An algorithmic introduction to numerical simulation of stochastic differential equations. *SIAM Rev.* 43:525–546.